



Universiteit
Leiden
The Netherlands

Viral gene therapy approaches for CRB1 retinal disease

Boon, N.

Citation

Boon, N. (2023, November 2). *Viral gene therapy approaches for CRB1 retinal disease*. Retrieved from <https://hdl.handle.net/1887/3655975>

Version: Publisher's Version

License: [Licence agreement concerning inclusion of doctoral thesis in the Institutional Repository of the University of Leiden](#)

Downloaded from: <https://hdl.handle.net/1887/3655975>

Note: To cite this publication please use the final published version (if applicable).

Chapter 5

Characterization and AAV-Mediated Gene Therapy in Human
Derived $CRB1^{KO}$ and $CRB1^{KO}CRB2^{+/-}$ Retinal Organoids

N. Boon, X. Lu, C. A. Andriessen, M. Orlova, P. M. J.
Quinn, C. J. F. Boon, and J. Wijnholds

Manuscript Submitted



Abstract

Using human induced pluripotent stem cell (hiPSC)-derived models for ophthalmology research is an emerging strategy to explore patient phenotypes *in vitro*, which allows access to previously limited or inaccessible material. The majority of patients with mutations in *CRB1* develop either early-onset retinitis pigmentosa as young children or Leber congenital amaurosis as newborns. The cause for the phenotypic variance exhibited in *CRB1*-associated inherited retinal diseases is unknown, but might be linked to differences in CRB1 and CRB2 protein levels in Müller glial and photoreceptor cells. Here, *CRB1*^{KO} and *CRB1*^{KO}*CRB2*^{+/-} hiPSC were generated by CRISPR/Cas9 and differentiated into retinal organoids. Differentiation day 210 retinal organoids showed a significant decrease in the number of photoreceptor nuclei in a row and a significant increase in the number of photoreceptor cell nuclei above the outer limiting membrane. This phenotype with outer retinal abnormalities is similar to previously observed in *CRB1* retinitis pigmentosa patient-derived retinal organoids and *Crb1* or *Crb2* mutant mouse retinal disease models. The *CRB1*^{KO} and *CRB1*^{KO}*CRB2*^{+/-} retinal organoids develop an additional inner retinal phenotype due to the complete loss of CRB1 from Müller glial cells, suggesting an essential role for CRB1 in proper localization of neuronal cell types in the inner and outer retina. AAV transduction was explored at early and late stages of organoid development. Moreover, AAV-mediated gene augmentation therapy with AAV.h*CRB2* improved the outer retinal phenotype in *CRB1*^{KO} retinal organoids partially. Altogether, these data provide essential information for future gene therapy approaches for patients with *CRB1*-associated retinal dystrophies.

Introduction

Crumbs homologue 1 (CRB1) is a large transmembrane protein initially discovered at the apical membrane of *Drosophila* epithelial cells [1]. The human *CRB1* gene is mapped to chromosome 1q31.3, has 12 identified mRNA transcripts, over 210 kb genomic DNA, and three CRB family members [2]. Canonical human CRB1 consists of multiple epidermal growth factor (EGF) and laminin-globular like domains in its

large extracellular domain. The short intracellular domain contains a FERM domain juxtaposed to the single transmembrane domain and at the carboxyl-terminus a conserved glutamic acid-arginine-leucine-isoleucine (ERLI) PDZ binding motive [2–4]. A short alternative transcript of *CRB1*, *CRB1-B*, was described encoding a protein with significant extracellular domain overlap with canonical CRB1 while bearing unique amino-terminal and carboxy-terminal protein domains [5]. The function of *CRB1-B* in the human retina is not known. In mammals, the CRB family members are CRB1, CRB2 and CRB3A. CRB2 displays a similar protein structure to CRB1, except for a depletion of four EGF domains. The canonical CRB complex is formed by interaction with protein associated with Lin Seven 1 (PALS1), which binds to the conserved carboxy-terminal PDZ domain of CRB [6–8]. The CRB complex is evolutionary conserved and is important for regulating apical-basal polarity and maintaining cell adhesion [9].

Inherited retinal dystrophies such as retinitis pigmentosa (RP) or Leber congenital amaurosis (LCA) can be caused by mutations in the *CRB1* gene. Approximately 7-17% of LCA and 3-9% of RP patients are reported with mutations in *CRB1* [10–13]. RP is a clinically and genetically heterogeneous disease where children or aged patients experience night blindness which progresses to complete loss of vision [14–16], while LCA causes visual impairment in newborns [13]. There are over 200 different mutations along the *CRB1* gene described to be causing early onset RP in children or LCA without a clear genotype-phenotype correlation [14,17]. No treatment possibilities are available for patients with a mutation in the *CRB1* gene. Multiple animal-derived models have been described that mimic the phenotype of *CRB1* patients [5,18–22]. However, recent immuno-electron microscopy studies have shown that the subcellular localization of CRB1 and CRB2 is different between rodents and humans [23]. In mice, CRB1 is located at the subapical region just above the outer limiting membrane (OLM) of Müller glial cells (MGC) while CRB2 is located at the subapical region of MGC and photoreceptor cells [24]. In adult non-human-primate retina, human-derived retinal organoids and human fetal retina, both CRB1 and CRB2 are located at the subapical region of MGC and photoreceptor cells [23]. In addition, a reappraisal of the phenotype-genotype correlation of 50 patients with regards to canonical CRB1 and the

photoreceptor-specific CRB1-B has shown that the retinal phenotype is mainly driven by canonical *CRB1* isoform impairment [25]. These data indicate thus the importance of using human-derived models to study the retinal dystrophy caused by mutations in *CRB1*.

The use of human-induced pluripotent stem cells (hiPSC)-derived models for research is an emerging strategy to explore patient organoid or cell phenotypes *in vitro*. This is specifically of interest for patients with mutations in *CRB1*, because the subcellular localization of the protein is different between rodents and humans. hiPSC can be differentiated into well-defined retinal organoids, which recapitulate the development of the fetal retina [23]. Previously, we have shown that *CRB1*-patient derived retinal organoids frequently show ectopic photoreceptor cells above the OLM and detected less variant CRB1 protein at the OLM of patient-derived retinal organoids at differentiation day 180 (DD180) and DD210 [23,26]. In a large clinical cohort, it is shown previously that there is no clear genotype-phenotype correlation for patients with a mutation in the *CRB1* gene and the mutations are distributed along the *CRB1* gene [14]. Here, we describe the use of hiPSC-derived *CRB1*^{KO} retinal organoids as a candidate model for Leber congenital amaurosis, where a single nucleotide was deleted by CRISPR/Cas9 in exon 2 resulting in a frameshift with a premature stop codon and thus a knockout of the gene of interest. In addition, *CRB1*^{KO}*CRB2*^{+/-} hiPSC were used, since previous research has shown that concomitant decreased levels of *CRB2* can exacerbate the phenotype in *CRB1* mutant mice [27–29]. Homozygous mutations were introduced by CRISPR/Cas9 in exon 2 of *CRB1* and a heterozygous mutation in exon 3 of *CRB2*, generating *CRB1*^{KO}*CRB2*^{+/-} hiPSC. *CRB* retinal organoids completely lacking CRB1 protein showed an outer and inner retina phenotype mimicking a mild form of LCA. *CRB1*^{KO} retinal organoids were used for adeno-associated viral vector (AAV)-mediated h*CRB1* or h*CRB2* gene augmentation therapy.

Results

Generation of $CRB1^{KO}$ and $CRB1^{KO}CRB2^{+/-}$ hiPSC from the isogenic control

From the control iPSC line LUMC4iCTRL10 (now called: ISO-4.10), three $CRB1^{KO}$ and three $CRB1^{KO}CRB2^{+/-}$ clones were generated using CRISPR-Cas9 technology (Applied StemCell). In short, guide RNAs were designed to target exon 2 of $CRB1$ and exon 3 of $CRB2$. For the $CRB1^{KO}$, three independent homozygous subclones (CL19, CL26, and CL72) carried a homozygous deletion (c.500del), resulting in a frameshift with premature stop p.(Ser44Serfs*) for the $CRB1$ gene (Supplemental Figure 1A). For $CRB1^{KO}CRB2^{+/-}$, two clones (CL4 and CL9) carried the same homozygous c.500del mutation and the CL17 iPSC clone carried a homozygous c.498_507delinsTGCC mutation in the $CRB1$ gene, both mutations result in a frameshift with premature translation stop of CRB1 (Supplemental Figure 1A).

For the $CRB2$ gene, the $CRB1^{KO}CRB2^{+/-}$ clones showed heterozygous mutations targeting exon 3 (Supplemental Figure 1B). Next Generation Sequencing (NGS) of the $CRB2$ gene showed for $CRB1^{KO}CRB2^{+/-}$ clones 4 and 9 a 23bp deletion in exon 3 of the $CRB2$ gene (Supplemental Figure 1B), resulting in a frameshift with an alternative translation of CRB2. $CRB1^{KO}CRB2^{+/-}$ clone 17 show a 2bp deletion in exon 3 of the $CRB2$ gene (Supplemental Figure 1B), resulting in a frameshift with an alternative translation of CRB2 and the normal protein translation. Karyotyping of all clones showed a normal karyotype (Supplemental Figure 1C, D), but the $CRB1^{KO}$ and $CRB1^{KO}CRB2^{+/-}$ showed a commonly observed gain in copy number variation on chromosome 20q (Supplemental Figure 1E). The biological significance of such recurrent abnormalities is still discussed [30], and further research is required to define this. These CRB and isogenic (ISO-4.10) hiPSC lines were differentiated into $CRB1^{KO}$, $CRB1^{KO}CRB2^{+/-}$, and isogenic control retinal organoids.

CRB1^{KO} and CRB1^{KO}CRB2^{+/-} retinal organoids show an inner retinal phenotype at DD210

The *CRB1^{KO}*, *CRB1^{KO}CRB2^{+/-}*, and isogenic control iPSC lines were differentiated into defined retinal organoids with outer segment like structures up to, at least, DD210 based on bright field images of the retinal organoids in culture (Figure 1A-C'). In addition, a laminated retina with a clear outer nuclear layer (ONL) marked by rhodopsin positive photoreceptor cells (Figure 1D) and an inner nuclear layer (INL) indicated with SOX9 positive MGCs and ISLET1-2 positive rod and ON-cone bipolar cells (Figure 1E) were observed in all retinal organoids at DD210. However, we observed a less defined alignment of SOX9 and ISLET1-2 positive cells in the inner retina of *CRB1^{KO}* and *CRB1^{KO}CRB2^{+/-}* compared with isogenic control retinal organoids, possibly due to the complete loss of canonical CRB1 in MGC (and photoreceptors). This was previously not observed in *CRB1* patient-derived retinal organoids that expressed strongly decreased but existing basic levels of variant CRB1 [23,26]. The data on the *CRB1^{KO}* and *CRB1^{KO}CRB2^{+/-}* retinal organoids at DD210 suggests the disrupted localization of rod and ON-cone bipolar cells. In summary, whereas in previous studies on *CRB1* patient-derived retinal organoids with missense mutations we observed disruptions of the photoreceptor layer, the *CRB1^{KO}* and *CRB1^{KO}CRB2^{+/-}* retinal organoids show at DD210 an extended retinal phenotype that includes disruptions of the inner retina.

CRB1^{KO} and CRB1^{KO}CRB2^{+/-} retinal organoids show an outer retinal phenotype at DD180 and DD210

To verify that the *CRB1^{KO}* mutation caused a complete loss of CRB1 protein expression, immunohistochemical staining of CRB1 on DD180 and DD210 isogenic control, *CRB1^{KO}*, and *CRB1^{KO}CRB2^{+/-}* retinal organoids was performed. CRB1 and MUPP1 staining at the OLM were observed in the isogenic control at DD180 (Figure 2A). No CRB1 staining was detected in *CRB1^{KO}* and *CRB1^{KO}CRB2^{+/-}* retinal organoids, whereas MUPP1 was detected at the OLM (Figure 2A). Both extracellular and intracellular CRB1 antibodies detected no CRB1 staining at the OLM of *CRB1^{KO}* and

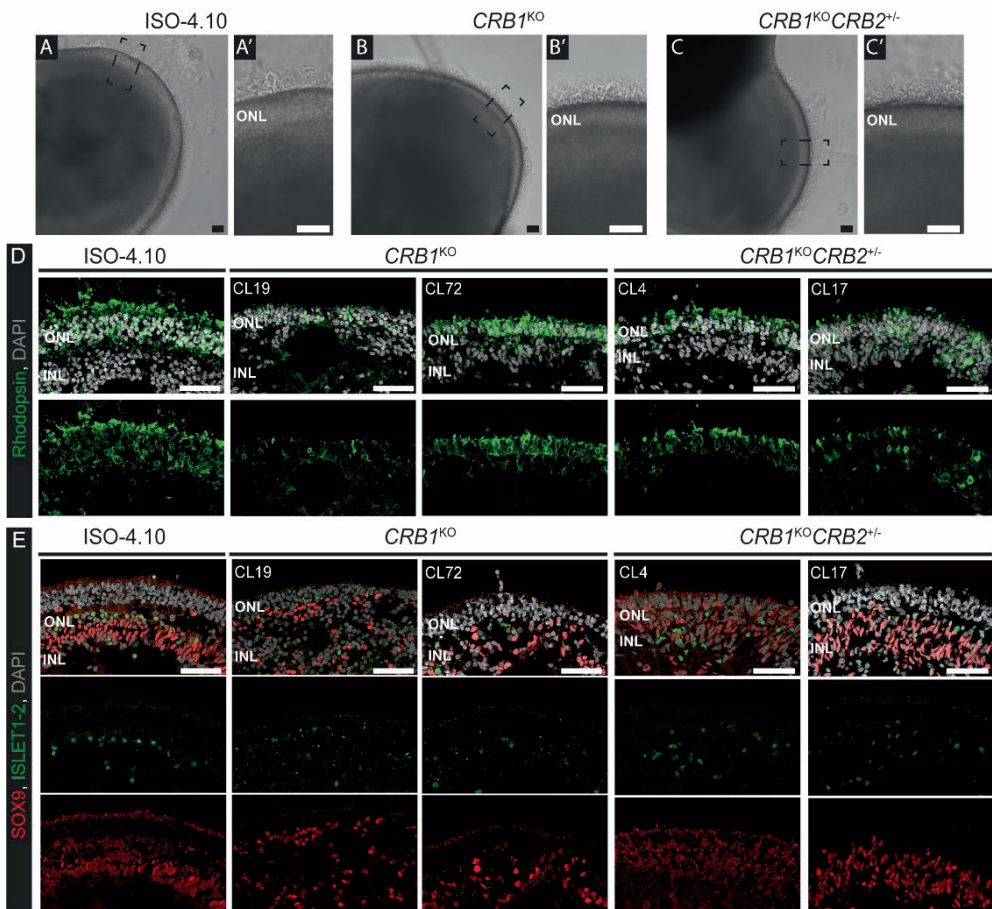


Figure 1: *CRB1*^{KO} and *CRB1*^{KO}*CRB2*^{+/-} retinal organoids at DD210. (A, B, C) Representative brightfield images of the (A) isogenic control and (B) *CRB1*^{KO} and (C) *CRB1*^{KO}*CRB2*^{+/-} retinal organoids at DD210, with a zoom-in of the outer segment-like structures in the boxed areas (A', B', C'). (D, E) Representative immunohistochemistry images of DD210 isogenic control and two *CRB1*^{KO} and *CRB1*^{KO}*CRB2*^{+/-} retinal organoids stained with (D) rhodopsin and (E) SOX9 (red) and ISLET1-2 (green). Note: INL = Inner Nuclear Layer, ONL = Outer Nuclear Layer. Scalebar = 50 μm.

CRB1^{KO}*CRB2*^{+/-} DD180 retinal organoids (Supplemental Figure 2A). Also, at DD210, no CRB1 was detected in *CRB1*^{KO} and *CRB1*^{KO}*CRB2*^{+/-} retinal organoids, whereas PALS1 was detected at the OLM (Supplemental Figure 2B). Moreover, CRB2 protein was detected at the OLM in DD180 and DD210 isogenic control, *CRB1*^{KO}, and

$CRB1^{KO}CRB2^{+/-}$ retinal organoids (Figure 2B, Supplemental Figure 2C). Localization of CRB2 was also detected at the OLM of $CRB1^{KO}CRB2^{+/-}$ retinal organoids that harbor one wild type and one knockout allele of $CRB2$.

When analyzing the $CRB1^{KO}$ and $CRB1^{KO}CRB2^{+/-}$ retinal organoids in more detail, a significantly increased number of photoreceptor nuclei above the OLM was observed compared to the isogenic control at DD180 (Figure 2C). Moreover, a statistically significant decrease in the number of photoreceptor nuclei in a row and ONL thickness was observed in DD180 $CRB1^{KO}$ and $CRB1^{KO}CRB2^{+/-}$ retinal organoids compared to the isogenic control (Figure 2D, Supplemental Figure 3A). No difference was observed for the INL thickness nor the retinal thickness in $CRB1^{KO}$ and $CRB1^{KO}CRB2^{+/-}$ retinal organoids (Supplemental Figure 3B, C). At DD210, the number of photoreceptor nuclei in a row was still significantly decreased in $CRB1^{KO}$ and $CRB1^{KO}CRB2^{+/-}$ retinal organoids (Figure 2E). However, there were fewer photoreceptor nuclei above the OLM in $CRB1^{KO}$ and $CRB1^{KO}CRB2^{+/-}$ retinal organoids, though still statistically significant for $CRB1^{KO}CRB2^{+/-}$ retinal organoids compared to the isogenic control (Figure 2F). Again, no statistically significant difference in INL thickness and retinal thickness was observed at DD210 (Supplemental Figure 3E, F). The data indicate that an outer retinal phenotype was observed at DD180 and DD210 retinal organoids, which is comparable to previously observed outer retinal phenotype in $CRB1$ patient-derived retinal organoids and in $Crb1$ mutant mouse models. Together these data define outcome measures for assessing therapeutic efficacy in $CRB1^{KO}$ and $CRB1^{KO}CRB2^{+/-}$ retinal organoids.

AAV5.CMV.GFP and AAV2.CMV.GFP transduce control retinal organoids more efficiently at DD135 than at DD200

Previously, we have shown that serotype AAV2/5.CMV.GFP (from now: AAV5.CMV.GFP) was more efficient than AAV2/2.CMV.GFP (from now: AAV2.CMV.GFP) in transducing MGC at DD120 [26]. Here, the tropism of these two serotypes were investigated in control retinal organoids transduced at later timepoints: DD135 or DD200.

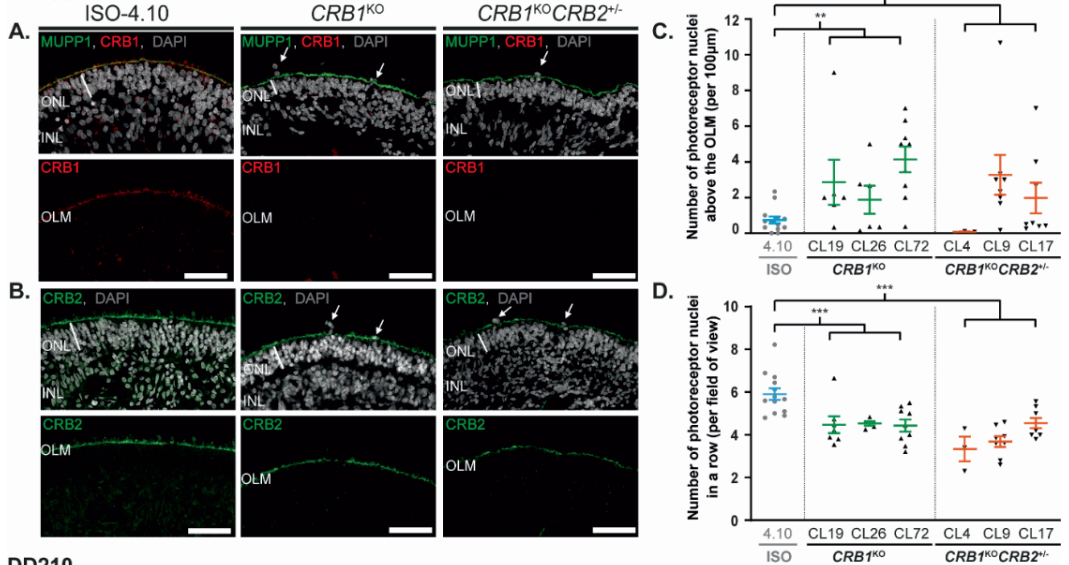
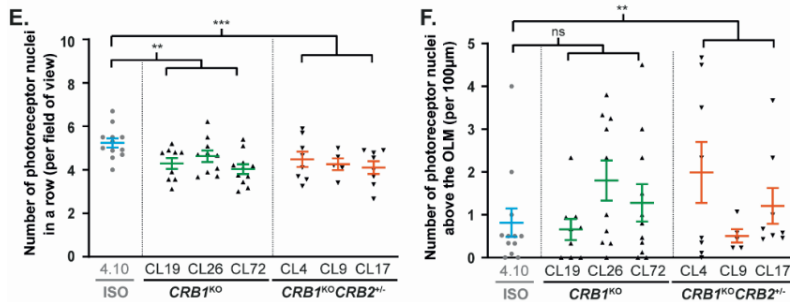
DD180

DD210


Figure 2: $CRB1^{KO}$ and $CRB1^{KO}CRB2^{+/-}$ retinal organoids show more photoreceptor nuclei above the OLM compared to the isogenic control at DD180 and DD210. Representative immunohistochemical images of (A) CRB1 (red) co-stained with MUPP1 (green) and (B) CRB2 (green) at the OLM of DD180 control, $CRB1^{KO}$, and $CRB1^{KO}CRB2^{+/-}$ retinal organoids. (C) Quantification of the number of photoreceptor nuclei above the OLM and (D) number of photoreceptor nuclei in a row of DD180 control, $CRB1^{KO}$, $CRB1^{KO}CRB2^{+/-}$ retinal organoids. (E) Quantification of the number of photoreceptor nuclei above the OLM and (F) number of photoreceptor nuclei in a row of DD210 control, $CRB1^{KO}$, $CRB1^{KO}CRB2^{+/-}$ retinal organoids. Each datapoint in the graph represents individual organoids, of which an average has been taken of at least three representative images. The standard error of mean (SEM) is derived from these averages. Number of individual organoids used for the quantification per condition at DD180: 4.10 $n=14$, $CRB1^{KO}$ CL19 $n=7$, CL26 $n=5$, CL72 $n=9$, $CRB1^{KO}CRB2^{+/-}$ CL4 $n=3$, CL9 $n=8$, CL17 $n=8$; and DD210: 4.10 $n=12$, $CRB1^{KO}$ CL19 $n=9$, CL26 $n=10$, CL72 $n=11$, $CRB1^{KO}CRB2^{+/-}$ CL4 $n=8$, CL17 $n=8$ from at least two independent differentiation batches and $CRB1^{KO}CRB2^{+/-}$ CL9 $n=5$ from one differentiation batch. Note: INL = Inner Nuclear Layer,

ONL = Outer Nuclear Layer, OLM = Outer Limiting Membrane. Scalebar = 50 μ m, statistical analysis: generalized linear mixed models with $p < 0.05$ (*), $p < 0.01$ (**), and $p < 0.001$ (***)

At DD135, control retinal organoids were transduced with 1×10^{10} gc, 6.6×10^{10} gc or 10×10^{10} gc of AAV2.CMV.*GFP* or AAV5.CMV.*GFP* and analyzed using immunohistochemistry after three weeks in culture. A dose-dependent increase of GFP positive cells was observed when control organoids were treated with AAV5.CMV.*GFP* or AAV2.CMV.*GFP* at DD135 (Figure 3A-C). The AAV-treated retinal organoids were quantified for the number of GFP positive cells in the ONL and INL. AAV2.CMV.*GFP* significantly transduced more cells in the ONL at the two highest titers (Figure 3D), whereas AAV5.CMV.*GFP* transduced significantly more cells in the INL at 6.6×10^{10} gc (Figure 3E). Co-staining with photoreceptor marker (OTX2) and MGC markers (CRALBP) confirmed the transduction of both cell types in AAV2.CMV.*GFP* as well as AAV5.CMV.*GFP* transduced organoids (Figure 3F, G). These data is in accordance with what was observed when control retinal organoids were transduced at DD120.

5
Next, we investigated whether transduction with the same AAV capsids at a later timepoint would influence the tropism. Here, control retinal organoids were transduced with 1×10^{10} gc or 10×10^{10} gc at DD200 with AAV2.CMV.*GFP* or AAV5.CMV.*GFP*. Again, a dose-dependent increase in GFP positive cells transduced in the ONL was observed for AAV2.CMV.*GFP* and AAV5.CMV.*GFP* treated retinal organoids (Supplemental Figure 4A, B). This dose-dependent increase was statistically significant for both capsids in the ONL (Supplemental Figure 4C) and only for AAV5.CMV.*GFP* in the INL (Supplemental Figure 4D). Moreover, AAV5.CMV.*GFP* infected significantly more cells in the ONL than AAV2.CMV.*GFP* at both titers (Supplemental Figure 4C). A small but statistically significant increase in GFP positive cells in the INL was observed at the dose of 10×10^{10} gc AAV5.CMV.*GFP* (Supplemental Figure 4D). However, the number of GFP positive cells co-localizing with SOX9-marked MGC cells showed no significant increase at the dose of 10×10^{10} gc AAV5.CMV.*GFP* (Supplemental Figure 4E). Both AAV serotypes showed co-localization with SOX9 positive MGCs (Supplemental Figure 4F). Interestingly, within relatively large retinal

organoids only a few cells were transduced with AAV2.CMV.GFP or with AAV5.CMV.GFP at DD200 (Supplemental Figure 4G), especially when compared with previous efficient transductions at DD120 [26] and DD135.

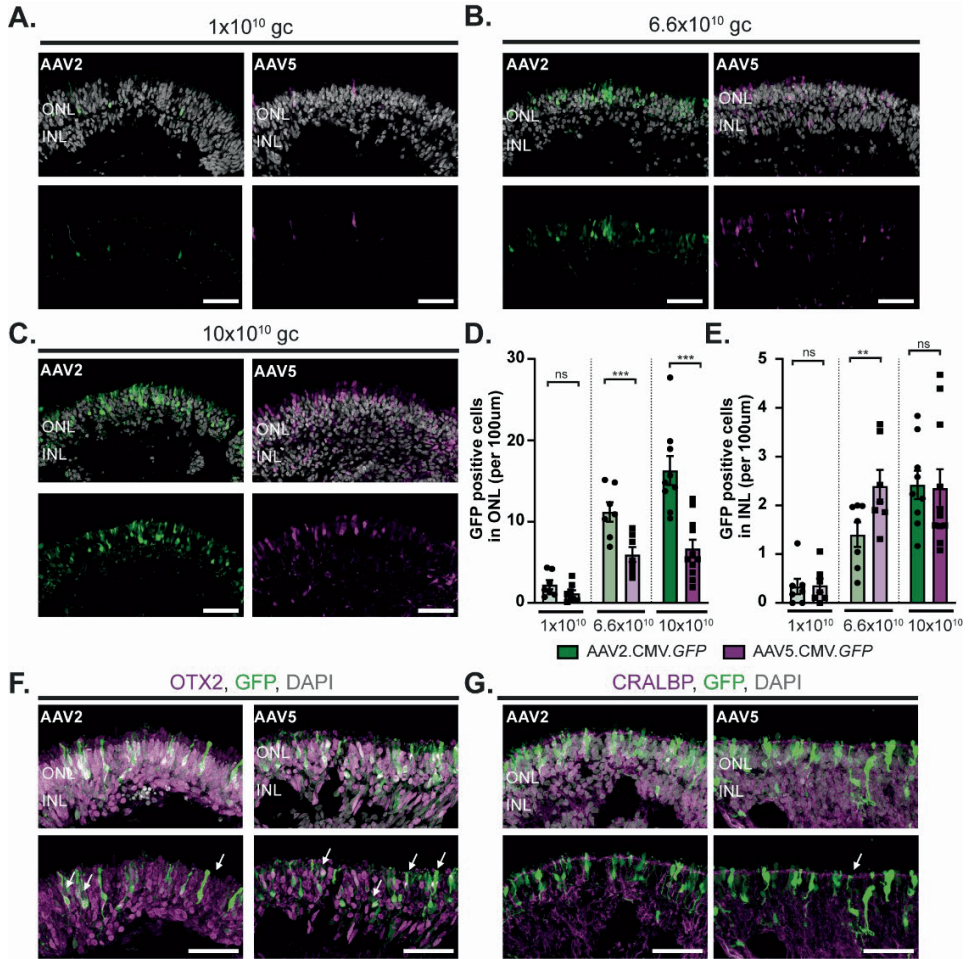


Figure 3: AAV transduction study of control retinal organoids transduced at DD135 with AAV2.CMV.GFP or AAV5.CMV.GFP (A, B, C) Representative immunohistochemical images of control retinal organoids transduced with (A) 1x10¹⁰gc, (B) 6.6x10¹⁰gc, or (C) 10x10¹⁰gc AAV2.CMV.GFP or AAV5.CMV.GFP. (D, E) Quantification of the number of GFP positive cells in the (D) ONL and (E) INL. (F, G) Immunohistochemical images of co-localization of AAV.GFP with photoreceptor marker OTX2 (F) or MGC marker CRALBP (G). Each datapoint in the graph represents individual organoids, of which an average has been taken of 3-6 representative images. The SEM is derived from these averages. Number of individual

organoids used for quantification per condition for AAV2.CMV.GFP: 1×10^{10} gc $n = 7$, 6.6×10^{10} gc $n = 7$, 10×10^{10} gc $n = 10$; and for AAV5.CMV.GFP: 1×10^{10} gc $n = 9$, 6.6×10^{10} gc $n = 7$, 10×10^{10} gc $n = 11$ from at least two independent differentiations. Note: INL = Inner Nuclear Layer, ONL = Outer Nuclear Layer. Scalebar = $50 \mu\text{m}$, statistical analysis: generalized linear mixed models with $p < 0.05$ (*), $p < 0.01$ (**), and $p < 0.001$ (***)

AAV-mediated CRB2 gene augmentation therapy improves the outer retinal phenotype in CRB1^{KO} retinal organoids

For gene therapy purposes, CRB1^{KO} retinal organoids were treated at DD120 with 3.3×10^{10} genome copies (gc) AAV5.CMV.hCRB1 or AAV5.CMV.hCRB2 (from now: AAV.hCRB1 and AAV.hCRB2, respectively) and subsequently analyzed at DD210 using immunohistochemistry. First, the isogenic control was treated with AAV.hCRB to determine whether there is a positive or negative effect of the gene therapy on control retinal organoids. No difference in retinal lamination or localization of MUPP1 at the OLM was observed after AAV.hCRB treatment of the isogenic control (Figure 4A, B, C). Also no statistically significant difference was observed after AAV.hCRB1 nor with AAV.hCRB2 treatment of the isogenic control for the number of photoreceptor nuclei in a row and the photoreceptor nuclei above the OLM (Figure 4D, E).

5

Next, AAV-mediated gene augmentation therapy was performed on three CRB1^{KO} iPSC lines differentiated into retinal organoids. AAV transduction was performed on two independent differentiation batches, one batch with and one without additional co-infection of 3.3×10^{10} gc AAV5.CMV.GFP. The results of both experiments were pooled. Immunohistochemical analysis at DD210 showed proper lamination and MUPP1 localization at the OLM after AAV.hCRB treatment (Figure 4A, B, C). AAV.hCRB1 and AAV.hCRB2 expression has been confirmed using immunohistochemistry at the OLM after AAV.hCRB treatment in CRB1^{KO} (Supplemental Figure 5A, B) and in CRB1 patient-derived retinal organoids [26]. A statistically significant increase in the number of photoreceptor nuclei in a row after AAV.hCRB2 treatment was observed for CRB1^{KO} CL19 and CL26 compared to the untreated CRB1^{KO} (Figure 4D). This improvement was more pronounced when the three CRB1^{KO} clones were combined (Figure 4E). In addition, a small, but not statistically significant, decrease in number of photoreceptor nuclei above the OLM

was observed after AAV.h*CRB2* treatment of the combined *CRB1*^{KO} retinal organoids (Figure 4G). No statistically significant improvement was observed after AAV.h*CRB1* treatment of *CRB1*^{KO} retinal organoids (Figure 4D-G, Supplemental Figure 5C-H). For the ONL thickness, retinal thickness, and INL thickness no statistically significant differences were observed with AAV.h*CRB* treatment of *CRB1*^{KO} retinal organoids (Supplemental Figure 5C-H). Altogether, the data show a partial improvement of the outer retinal phenotype of *CRB1*^{KO} retinal organoids after treatment with AAV.h*CRB2* in DD210 retinal organoids.

Discussion

In this study, we have shown that the complete loss of CRB1 in human *CRB1*^{KO} and *CRB1*^{KO}*CRB2*^{+/-} retinal organoids results in degeneration of the inner and outer retina, whereas *CRB1* retinitis pigmentosa patient-derived retinal organoids carrying a missense mutation showed strongly reduced levels of variant CRB1 and degeneration of the outer retina [23,26]. We also show that AAV transduction efficiency of retinal organoids depends on the time point of retinal organoid development. In addition, a partially improved outer retina phenotype of *CRB1*^{KO} retinal organoids was observed after AAV.h*CRB2* transduction.

Here, in order to generate a model for a mild form of LCA, CRISPR/Cas9 was used to generate *CRB1*^{KO} iPSC with a nucleotide deletion in exon 2 of the *CRB1* gene. The nucleotide deletion caused a frameshift resulting in a premature protein translation stop codon. Immunohistochemical analysis confirmed the complete loss of CRB1 in *CRB1*^{KO} retinal organoids at DD180 and DD210. A decreased number of photoreceptor nuclei in a row in the ONL and an increased number of photoreceptor cell nuclei above the OLM were observed at DD180 and DD210 in *CRB1*^{KO} retinal organoids compared to the isogenic control. The data are similar to what was previously observed in *CRB1* retinitis pigmentosa patient-derived retinal organoids carrying missense mutations that allow the expression of a variant CRB1 protein [26]. Moreover, the complete loss of

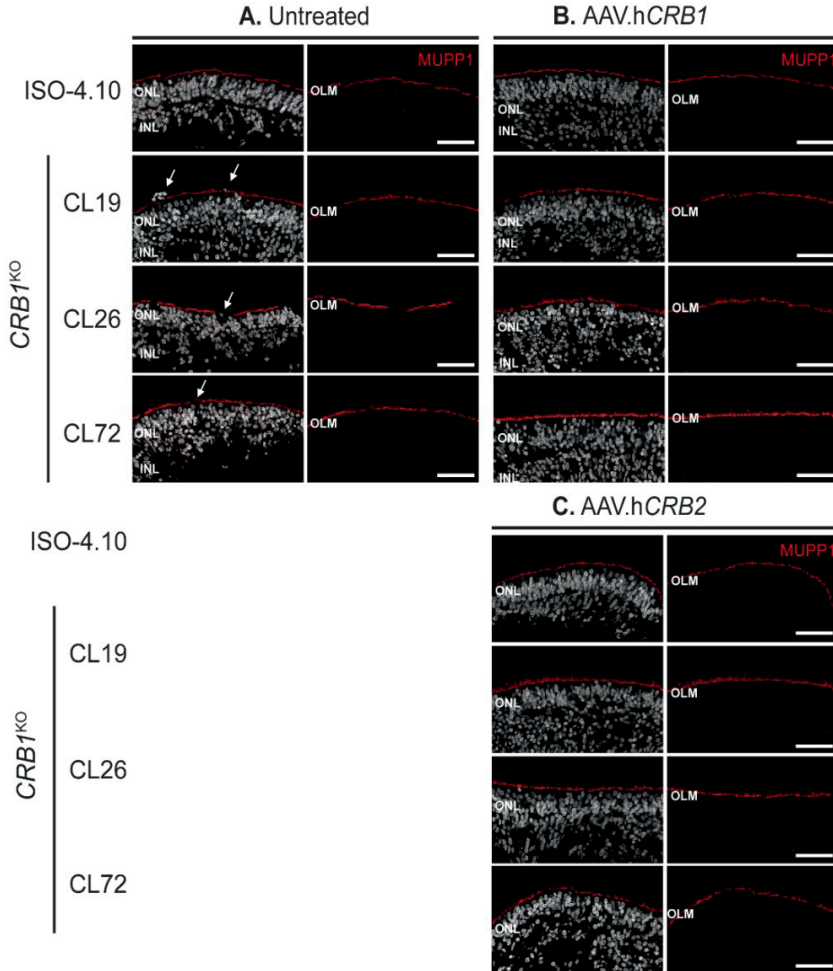


Figure 4 (A-C): AAV-mediated gene therapy on $CRB1^{KO}$ organoids shows an improved number of photoreceptor nuclei in a row. (A, B, C) Representative immunohistochemical images of (A) untreated, (B) AAV.hCRB1, or (C) AAV.hCRB2 treated control and $CRB1^{KO}$ retinal organoids at DD120 and analysed at DD210. Stained with MUPP1 (red) at the OLM.

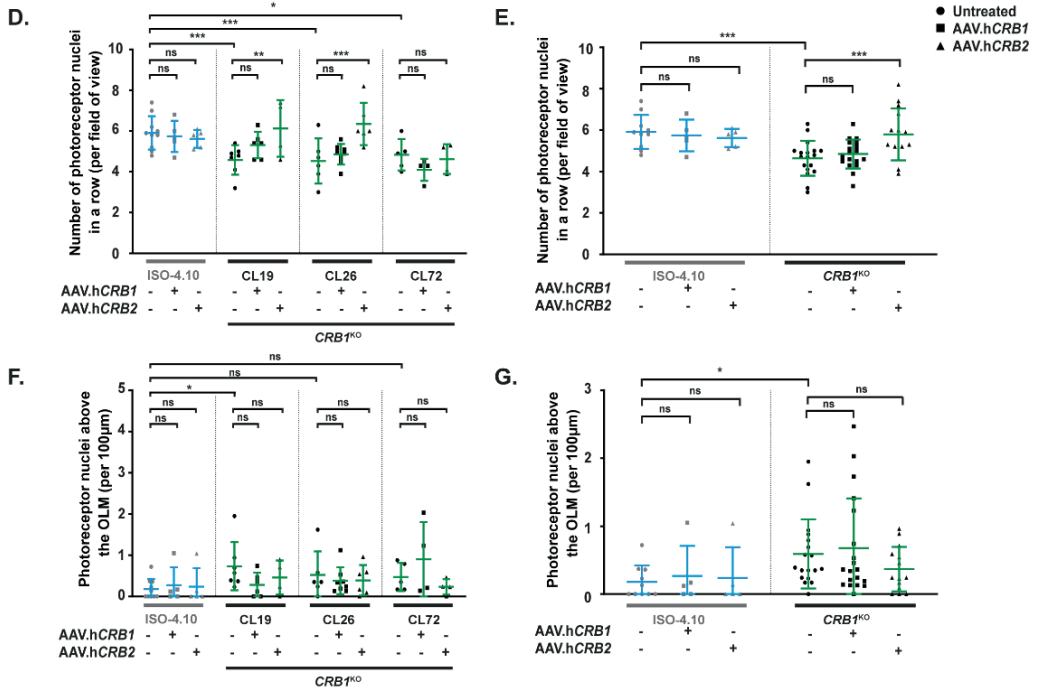


Figure 4 (D-G): AAV-mediated gene therapy on $CRB1^{KO}$ organoids shows an improved number of photoreceptor nuclei in a row. (D, E, F, G) Quantification of the number of photoreceptor nuclei in a row (D, E) and above the OLM (F, G) per $CRB1^{KO}$ clone (D, F) or all $CRB1^{KO}$ clones combined (E, G). Each datapoint in the graph represent an individual organoid, of which an average has been taken of at least three representative images. The SEM is derived from these averages. Number of individual organoids used for quantification per condition for untreated: 4.10 $n = 10$, $CRB1^{KO}$ CL19 $n = 7$, CL26 $n = 7$, CL72 $n = 5$; AAV.hCRB1 treated: 4.10 $n = 5$, $CRB1^{KO}$ CL19 $n = 6$, CL26 $n = 8$, CL72 $n = 4$ from two independent differentiation batches; and AAV.hCRB2 treated: 4.10 $n = 5$, $CRB1^{KO}$ CL19 $n = 4$, CL26 $n = 6$, CL72 $n = 3$ from one differentiation batch. Note: INL = Inner Nuclear Layer, ONL = Outer Nuclear Layer, OLM = Outer Limiting Membrane. Scalebar = 50µm, statistical analysis: generalized linear mixed models with $p < 0.05$ (*), $p < 0.01$ (**), and $p < 0.001$ (***)

CRB1 in MGC of *Crb1* mouse retina also results in the protrusion of photoreceptor cell bodies into the subretinal space [7,31]. A more severe retinal phenotype in $CRB1^{KO}$ mice was observed with concomitant loss of *Crb2* in MGC [22,32], so this was investigated as well in the $CRB1^{KO}CRB2^{+/-}$ human retinal organoid model. A heterozygous mutation in *CRB2* targeting exon 3 was introduced in combination with a mutation targeting exon 2 of the *CRB1* gene, resulting in $CRB1^{KO}CRB2^{+/-}$ retinal organoids. These retinal

organoids show a similar outer retina phenotype as the *CRB1*^{KO} and *CRB1* patient-derived retinal organoids [26]. Interestingly, the *CRB1*^{KO} and *CRB1*^{KO}*CRB2*^{+/-} outer retina phenotypes studied here seem to be not much more severe than the outer retina phenotype previously observed in *CRB1* retinitis pigmentosa patient-derived retinal organoids [23,26]. The retinal organoids can show a variability in phenotype which can be caused by differences in genetic background, developmental age of the organoid or practical handling differences between researchers during the organoid culture. To exclude differences in genetic background, the *CRB1* and *CRB1*^{KO}*CRB2*^{+/-} knockout mutations needs to be introduced into the isogenic *CRB1* RP patient hiPSC. This will allow for a direct comparison between *CRB1* RP patient and *CRB1*^{KO} and *CRB1*^{KO}*CRB2*^{+/-} retinal organoids with their isogenic controls all on the same genetic background. Furthermore, then the retinal organoids need to be cultured at the same time under the same culturing conditions in multiple batches of differentiation.

5 Interestingly, an inner and outer retinal phenotype was observed in *CRB1*^{KO} and *CRB1*^{KO}*CRB2*^{+/-} retinal organoids compared to the isogenic control. This inner retinal phenotype was previously not observed in three independent *CRB1* retinitis pigmentosa patient-derived retinal organoids compared to their isogenic controls [23,26]. Staining for ISLET1/2-positive rods and ON-cone bipolar cells and SOX9-positive MGCs showed abnormal localization of these cell types in the INL of *CRB1*^{KO} and *CRB1*^{KO}*CRB2*^{+/-} retinal organoids. The data suggest that a complete lack of CRB1 in MGC and photoreceptors can result in a more advanced LCA-like phenotype affecting inner and outer retina. Interestingly, scRNA-seq analysis on DD230 *CRB1* patient-derived retinal organoids showed differences in gene expression profiles of MGC and photoreceptors, but changes were not detected in inner retinal cell types [26]. Future scRNA-seq studies on *CRB1*^{KO} and *CRB1*^{KO}*CRB2*^{+/-} retinal organoids with their isogenic controls might provide insight in changes in the inner and outer retina. Moreover, the *CRB1* retinitis pigmentosa patient-derived retinal organoids had missense mutations and surprisingly showed a strong reduction in levels of variant CRB1 protein, whereas the *CRB1* mRNA transcript levels were not changed [26]. The *CRB1*^{KO} and *CRB1*^{KO}*CRB2*^{+/-} retinal organoids showed complete loss of CRB1 leading to an inner and outer retina phenotype. scRNA-seq revealed that human MGC and

photoreceptors express relatively high levels of *CRB1* transcripts, and that photoreceptors express relatively high levels of *CRB2* while the MGCs express relatively low levels of *CRB2* [26]. We hypothesize that relatively low levels of human *CRB2* in MGC are the cause for the phenotype in the inner retina of *CRB1*^{KO} retinal organoids. But, interestingly, mouse retinas that solely lack either *CRB1* or *CRB2* in MGC show very mild RP outer retinal phenotypes [7,29,31] whereas a severe LCA-like retinal phenotype affecting inner and outer retina occurs in mouse retinas that lack both *CRB1* and *CRB2* in MGC [18]. Patients with missense variations in the *CRB1* gene can develop either early-onset RP or LCA or macular dystrophy [14,17]. Future studies need to show whether these differences in retinal phenotypes are due to relatively low levels of *CRB2* and variant *CRB1* in MGC.

All of the *CRB1*^{KO} and *CRB1*^{KO}*CRB2*^{+/-} iPSC, but not the isogenic control iPSC from which the *CRB* mutant lines were derived, contained a copy number variation (CNV) gain in chromosome 20q. This gain in chromosome 20q is one of the most common recurrent abnormalities in iPSCs and the biological significance of such recurrent abnormalities is still discussed [27]. Novel insights of CNV gains at 20q11.21 show that the differential gene expression pattern had a negative effect on the differentiation potential [33]. Genes associated with PI3K/AKT signaling pathway were significantly downregulated in the iPSC with a CNV gain at chromosome 20q, this pathway has an essential role in the survival of human pluripotent stem cells [33]. In our case, differentiating the *CRB1*^{KO} and *CRB1*^{KO}*CRB2*^{+/-} hiPSC into retinal organoids was more challenging than for the isogenic control. However, this could also be due to the quality of medium compounds (for example Matrigel), or other culture conditions, since we experienced this as well with other iPSC lines. Other groups also described the variability in the efficiency of differentiating certain iPSC lines efficiently into retinal organoids [34]. Therefore, more research is needed if this CNV can have a negative effect on the differentiation potential into retinal organoids.

AAV tropism at two differentiation days was compared. Mainly photoreceptor cells and MGC were transduced on DD135 and DD200 retinal organoids with either AAV2.CMV.*GFP* or AAV5.CMV.*GFP*. Similar transduction was previously observed

at DD120 and DD220 [23,26]. In conclusion, we have shown that AAV2/2 and AAV2/5 are capable of infecting MGC and photoreceptor cells in hiPSC-derived control retinal organoids.

Using AAV-mediated gene augmentation therapy we have partially improved the outer retinal phenotype in $CRB1^{KO}$ retinal organoids after AAV.h*CRB2* treatment. However, we did not observe a statistically significant improved number of photoreceptor nuclei in a row after AAV.h*CRB1* treatment of $CRB1^{KO}$ retinal organoids. The AAV.h*CRB1* vector contains a minimal CMV promoter, whereas the AAV.h*CRB2* vector contains a full-length CMV promoter. The short CMV promoter worked efficiently in mouse retina [35], but the promoter activities might differ in human MGCs and photoreceptors. In patient *CRB1* retinal organoids a statistically significant improved number of photoreceptor nuclei in a row in the ONL was observed after treatment with AAV.h*CRB1* and with AAV.h*CRB2* [26]. This could potentially be explained by the difference in low expression of a variant CRB1 protein in *CRB1* patient-derived retinal organoids and the complete absence of CRB1 protein expression in the $CRB1^{KO}$ retinal organoids. We hypothesize that the $CRB1^{KO}$ retinal organoids might need higher levels of AAV.h*CRB1* in MGCs to improve the outer retinal phenotype. Another possibility, as described above, could be because of modifying factors and differences in the genetic background. $CRB1^{KO}$ retinal organoids showed a partially improved retinal phenotype after AAV.h*CRB2* treatment. Using anti-CRB2 immunohistochemical staining recombinant h*CRB2* protein was detected at the OLM.

In conclusion, we generated and differentiated $CRB1^{KO}$ and $CRB1^{KO}CRB2^{+/-}$ hiPSC into retinal organoids and observed an extended phenotype compared to the phenotype observed in *CRB1*-patient derived retinal organoids and in *Crb* mutant mouse studies. The $CRB1^{KO}$ and $CRB1^{KO}CRB2^{+/-}$ retinal organoids showed an inner and outer retinal phenotype, whereas the *CRB1* patient-derived retinal organoids showed only an outer retinal phenotype. Using AAV-mediated gene augmentation therapy we have partially improved the outer retinal phenotype in $CRB1^{KO}$ retinal organoids. These data provide essential information for future gene therapy approaches for patients with mutations in the *CRB1* gene.

Experimental procedures

Generation of $CRB1^{KO}$ and $CRB1^{KO}CRB2^{+/-}$ hiPSC

Three $CRB1^{KO}$ (CL19, CL26, and CL72) and three $CRB1^{KO}CRB2^{+/-}$ (CL4, CL9, and CL17) were generated from the isogenic control (LUMC04iCTRL10) using CRISPR/Cas9 technology (Supplemental Table 1) (Applied Stem Cell, California, USA). In short, two guide RNAs (gRNA) per gene of interest were designed, targeting exon 2 of $CRB1$ and exon 3 of $CRB2$. These gRNAs were individually cloned into a gRNA/Cas9 expression vector by inserting double-stranded oligo cassettes of each gRNA between the two BbsI sites in the pBT-U6-Cas9-2A-GFP vector. Each oligo cassette consists of a 20bp gRNA sequence with a guanosine at the 5'-end for optimal expression, and adherent ends for cloning at BbsI sites. Following construct delivery into the target cells, the abilities of these gRNAs to promote double stranded breaks were evaluated using Sanger sequencing. gRNAs with the best targeting and repairing efficiency per gene of interest were selected for transfection of iPSC, gRNA for $CRB1$ = GAAACTACCATTGGTTCCTG and for $CRB2$ = AGAGCCAGCCGTGCG CACAT. After transfecting gRNA and Cas9 into the target cells, single cell-derived clones were screened and three correct clones per gene of interest were selected and expanded for further use. Confirmation of the mutation was done by PCR and subsequent sanger sequencing.

Confirmation of the mutation was done by PCR and subsequent sanger sequencing for $CRB1$ and NGS for $CRB2$ (Supplemental Table 2).

Next generation sequencing sample preparation and data analysis

Genomic DNA of hiPSC LUMC0004iCTRL10, and three $CRB1^{KO}CRB2^{+/-}$ (CL4, CL9, and CL17) were extracted using the DNeasy Blood & Tissue Kit protocol (Qiagen; 69506). The NGS first round PCR for $CRB2$ (Supplemental Table 2), to amplify a target region with Illumina adapter overhang, was performed using a GoTaq® G2 DNA Polymerase kit (Promega; M7845). After this, amplicons were purified by the AMPure XP kit (Beckman Coulter; A63881). Then the barcode PCR was performed to generate

a library of amplicons using Illumina tag-specific primer pairs with unique sequence combinations for demultiplexing and sample identification (Supplemental Table 3) using Kapa HiFi 2x Ready Mix (Roche; KK2602) and subsequently the purification using AMPure XP kit was carried out. The concentration was determined using Qubit2.0 fluorometer (Invitrogen) and Qubit dsDNA HS assay kit (Invitrogen; Q32854). The sample quality control was performed using capillary electrophoresis with a 2100 BioAnalyzer (Agilent). The amplicons from each sample were pooled at equivalent DNA quantities. Finally, this library of pooled barcoded amplicons was subjected to Illumina MiSeq sequencing with 100k reads. The data were analyzed using CRISPResso2 [38,39].

Cell culture and retinal organoid differentiation

The following hiPSC lines were used for organoid differentiation: three *CRB1*^{KO} (CL19, CL26, and CL72) and three *CRB1*^{KO}*CRB2*^{+/-} (CL4, CL9, and CL17) derived from the isogenic control (LUMC04iCTRL10) (Supplemental Table 1). hiPSC lines were derived from skin fibroblasts using polycistronic Lentiviral vectors [36]. hiPSC were cultured on Matrigel coated plates in mTeSR plus medium (STEMCELL Technologies) and passaged mechanically using gentle cell dissociation reagent. Retinal organoid differentiation was carried out as previously reported [26,37].

AAV transduction of hiPSC-derived retinal organoids

Two to three retinal organoids were plated in a single 96-well agarose coated plate, multiple 96-wells were used per experiment, and were infected at DD120, DD135 or DD200 with the appropriate AAV concentration in 50 μ L RLM2. Treated organoids were incubated at 5% CO₂ at 37°C and 8h later the organoids were topped up to 200 μ L. The next day, the treated organoids were transferred to a 24 well plate and cultured until the desired differentiation day (for AAV.*CRB* treatment) or for three weeks (for AAV.*GFP* tropism). The following viral vectors were used: AAV2/2.CMV.*GFP* (105530-AAV2; Addgene), AAV2/5.CMV.*GFP* (105530-AAV5; Addgene), AAV5.CMVmin.h*CRB1* and AAV5.CMV.h*CRB2* (HORAMA) with a titer of 1×10^{10} , 3.3×10^{10} , 6.6×10^{10} , or 10×10^{10} genome copies (gc) per well.

Immunohistochemical analysis

Organoids were collected and fixed with 4% paraformaldehyde in PBS for 20 minutes at room temperature (RT). Then briefly washed in PBS and subsequently cryo-protected in 15% and 30% sucrose for at least 30 minutes. The samples were embedded in Tissue-Tek O.C.T. Compound (Sakura, Finetek) and stored at -20°C for future use. Then cryosections of 8 μM were made with a Leica CM1900 cryostat (Leica Microsystems). Slides with cryosections were stored at -20°C for future use.

For the immunohistochemical analysis, the slides were blocked in 10% normal goat serum, 0.4% Triton X-100, and 1% bovine serum albumin in PBS for 1h at RT. Primary antibodies were incubated for least 3h at RT or overnight at 4°C with 0.3% normal goat serum, 0.4% Triton X-100, 1% BSA and appropriate primary antibody concentration. Slides were washed twice in PBS, and incubated with a secondary antibody in 0.1% goat serum in PBS for 1h at RT. Slides were then washed twice again in PBS, and mounted using Vectashield Hardset with DAPI mounting medium (H1800, Vector Laboratories, Burlingame, USA). The slides were imaged on a Leica TCS SP8 confocal microscope and images were processed using Leica Application Suite X (v3.7.0.20979).

The following primary antibodies were used: CRB1 AK2 (1:200; homemade = CRB1^{INT}, used for CRB1 if not otherwise specified), CRB1^{EX} (1:200, Abnova H00023418-A01), CRB2 SK11 (1:200; homemade), PALS1 (1:200; homemade), rhodopsin (1:500; Millipore Cat# MAB5356), SOX9 (1:250; Millipore Cat# AB5535), ISLET1-2 (1:200, DSHB Developmental Studies Hybridoma Bank 39.4D5-c Islet-1 & Islet-2 homeobox), MUPP1 (1:200, BD Biosciences M98820), OTX2 (1:200, Proteintech 13497-1-AP), CRALBP (1:200, Abcam Ab15051).

The following secondary antibodies were used; goat anti-mouse, goat anti-rabbit, or goat anti-chicken IgGs conjugated to Alexa 488, Alexa555, Alexa647 (1:1000, Abcam).

Quantification and statistical analysis

40x magnification images were manually quantified using Fiji ImageJ (ImageJ 1.53f51). At least 4 organoids from at least two differentiation batches per condition with 3-6 representative images of each organoid were used for quantification. The exact number of organoids used per experiment is mentioned in the figure legends. In each image, three regions were quantified for the number of photoreceptor nuclei in a row, the number of protruding cells above the OLM, the retinal thickness, INL thickness, and ONL thickness. All measured datapoints were averaged per organoid and plotted in the graph; so that each dot is one organoid. Data was either presented per 100µm retinal length or per field of view. Data presentation was performed using GraphPad Prism version 8 (GraphPad Software).

Statistical analysis was performed using IBM SPSS statistics (version 25). A generalized mixed model with treatment as a fixed effect was performed on all quantification parameters; all individual data points per image were used for statistical analysis. Each datapoint in the graph represents individual organoids, of which an average has been taken of 3-6 representative images. The standard error of the mean (SEM) is derived from these averages. Significance is indicated in graphs as $p < 0.05$ (*), $p < 0.01$ (**), and $p < 0.001$ (***)

5

Article information

Author contributions: Conceptualization, N.B. and J.W.; Formal analysis, N.B.; Investigation, N.B., X.L., C.A.A, M.O, and P.M.J.Q.; Data curation, N.B.; Writing - original draft, N.B.; Writing - review & editing, N.B, C.J.F.B, and J.W.; Visualization, N.B.; Supervision, J.W.; Project administration, J.W.; Funding acquisition, J.W.

Funding: This work was funded by The Netherlands Organization for Health Research and Development (ZonMw grant 43200004, to JW), research grant MDBR-19-131-CRB1 from the University of Pennsylvania Orphan Disease Center in partnership with the Curing Retinal Blindness Foundation (to JW), Bontius Stichting 32072-8231, and HORAMA 41400-8231.

Acknowledgements: The authors would like to thank Chelsey Linnenbank for technical assistance, the LUMC light and electron microscope facility for help during image acquisition, and all the previous and current members of the Wijnholds lab for advice on experiments and the manuscript.

Abbreviations:

AAV	Adeno-associated viral vectors
CRB1	Crumbs homolog-1
CNV	Copy number variation
CMV	Cytomegalovirus
DD210	Differentiation day 210
EGF	Epidermal growth factor
ERLI	Glutamic acid-arginine-leucine-isoleucine
GFP	Green Fluorescent Protein
gRNA	Guide RNA
hiPSC	Human-induced pluripotent stem cell
INL	Inner nuclear layer
LCA	Leber congenital amaurosis
MGC	Müller glial cell
MUPP1	Multiple PDZ domain protein 1
NGS	Next Generation Sequencing
OLM	Outer limiting membrane
ONL	Outer nuclear layer
PALS1	Protein associated with Lin Seven 1
RP	Retinitis pigmentosa
RT	Room temperature
SEM	Standard error of mean
SOX9	SRY-Box Transcription Factor 9

References

1. Tepass, U.; Theres, C.; Knust, E. crumbs encodes an EGF-like protein expressed on apical membranes of Drosophila epithelial cells and required for organization of epithelia. *Cell* **1990**, 61, 787–799, doi:10.1016/0092-8674(90)90189-L.
2. Den Hollander, A.I.; Ten Brink, J.B.; De Kok, Y.J.M.; Van Soest, S.; Van Den Born, L.I.; Van Driel, M.A.; Van De Pol, D.J.R.; Payne, A.M.; Bhattacharya, S.S.;

Kellner, U.; et al. Mutations in a human homologue of *Drosophila* crumbs cause retinitis pigmentosa (RP12). *Nat. Genet.* **1999**, *23*, 217–221, doi:10.1038/13848.

3. Boon, N.; Wijnholds, J.; Pellissier, L.P. Research Models and Gene Augmentation Therapy for CRB1 Retinal Dystrophies. *Front. Neurosci.* **2020**, *14*, 1–13, doi:10.3389/fnins.2020.00860.

4. Quinn, P.M.; Pellissier, L.P.; Wijnholds, J. The CRB1 complex: Following the trail of crumbs to a feasible gene therapy strategy. *Front. Neurosci.* **2017**, *11*, doi:10.3389/fnins.2017.00175.

5. Ray, T.A.; Cochran, K.; Kozlowski, C.; Wang, J.; Alexander, G.; Cady, M.A.; Spencer, W.J.; Ruzycki, P.A.; Clark, B.S.; Laeremans, A.; et al. Comprehensive identification of mRNA isoforms reveals the diversity of neural cell-surface molecules with roles in retinal development and disease. *Nat. Commun.* **2020**, *11*, doi:10.1038/s41467-020-17009-7.

6. Margolis, B. The Crumbs3 polarity protein. *Cold Spring Harb. Perspect. Biol.* **2018**, *10*, 1–9, doi:10.1101/cshperspect.a027961.

7. van de Pavert, S.A.; Kantardzhieva, A.; Malysheva, A.; Meuleman, J.; Versteeg, I.; Levelt, C.; Klooster, J.; Geiger, S.; Seeliger, M.W.; Rashbass, P.; et al. Crumbs homologue 1 is required for maintenance of photoreceptor cell polarization and adhesion during light exposure. *J. Cell Sci.* **2004**, *117*, 4169–4177, doi:10.1242/jcs.01301.

8. Roh, M.H.; Makarova, O.; Liu, C.J.; Shin, K.; Lee, S.; Laurinec, S.; Goyal, M.; Wiggins, R.; Margolis, B. The Maguk protein, Pals1, functions as an adapter, linking mammalian homologues of crumbs and discs lost. *J. Cell Biol.* **2002**, *157*, 161–172, doi:10.1083/jcb.200109010.

9. Bulgakova, N.A.; Knust, E. The Crumbs complex: From epithelial-cell polarity to retinal degeneration. *J. Cell Sci.* **2009**, *122*, 2587–2596, doi:10.1242/jcs.023648.

10. Vallespin, E.; Cantalapiedra, D.; Riveiro-Alvarez, R.; Wilke, R.; Aguirre-Lamban, J.; Avila-Fernandez, A.; Lopez-Martinez, M.A.; Gimenez, A.; Trujillo-Tiebas, M.J.; Ramos, C.; et al. Mutation screening of 299 Spanish families with retinal dystrophies by leber congenital amaurosis genotyping microarray. *Investig. Ophthalmol. Vis. Sci.* **2007**, *48*, 5653–5661, doi:10.1167/iovs.07-0007.

11. Bujakowska, K.; Audo, I.; Mohand-Säid, S.; Lancelot, M.E.; Antonio, A.; Germain, A.; eveillard, T.Ł.; Letexier, Melanie; Saraiva, J.P.; Lonjou, C.; et al. CRB1 mutations in inherited retinal dystrophies. *Hum. Mutat.* **2012**, *33*, 306–315, doi:10.1002/humu.21653.

12. Corton, M.; Tatu, S.D.; Avila-Fernandez, A.; Vallespín, E.; Tapias, I.; Cantalapiedra, D.; Blanco-Kelly, F.; Riveiro-Alvarez, R.; Bernal, S.; García-Sandoval, B.; et al. High frequency of CRB1 mutations as cause of Early-Onset Retinal

Dystrophies in the Spanish population. *Orphanet J. Rare Dis.* **2013**, 8, doi:10.1186/1750-1172-8-20.

13. Den Hollander, A.I.; Davis, J.; Van Der Velde-Visser, S.D.; Zonneveld, M.N.; Pierrottet, C.O.; Koenekoop, R.K.; Kellner, U.; Van Den Born, L.I.; Heckenlively, J.R.; Hoyng, C.B.; et al. *CRB1* mutation spectrum in inherited retinal dystrophies. *Hum. Mutat.* **2004**, 24, 355–369, doi:10.1002/humu.20093.

14. Talib, M.; van Schooneveld, M.J.; van Genderen, M.M.; Wijnholds, J.; Florijn, R.J.; ten Brink, J.B.; Schalijs-Delfos, N.E.; Dagnelie, G.; Cremers, F.P.M.; Wolterbeek, R.; et al. Genotypic and Phenotypic Characteristics of *CRB1*-Associated Retinal Dystrophies: A Long-Term Follow-up Study. *Ophthalmology* **2017**, 124, 884–895, doi:10.1016/j.ophtha.2017.01.047.

15. Verbakel, S.K.; van Huet, R.A.C.; Boon, C.J.F.; den Hollander, A.I.; Collin, R.W.J.; Klaver, C.C.W.; Hoyng, C.B.; Roepman, R.; Klevering, B.J. Non-syndromic retinitis pigmentosa. *Prog. Retin. Eye Res.* **2018**, 66, 157–186, doi:10.1016/j.preteyeres.2018.03.005.

16. Nguyen, X.; Moekotte, L.; Plomp, A.S.; Bergen, A.A.; Genderen, M.M. Van; Boon, C.J.F. Retinitis Pigmentosa: Current Clinical Management and Emerging Therapies. *Int. J. Mol. Sci.* **2023**, 24.

17. Talib, M.; Van Cauwenbergh, C.; De Zaeytijd, J.; Van Wynsberghe, D.; De Baere, E.; Boon, C.J.F.; Leroy, B.P. *CRB1*-Associated retinal dystrophies in a Belgian cohort: Genetic characteristics and long-Term clinical follow-up. *Br. J. Ophthalmol.* **2022**, 106, 696–704, doi:10.1136/bjophthalmol-2020-316781.

18. Quinn, P.M.; Mulder, A.A.; Henrique Alves, C.; Desrosiers, M.; de Vries, S.I.; Klooster, J.; Dalkara, D.; Koster, A.J.; Jost, C.R.; Wijnholds, J. Loss of *CRB2* in Müller glial cells modifies a *CRB1*-associated retinitis pigmentosa phenotype into a Leber congenital amaurosis phenotype. *Hum. Mol. Genet.* **2019**, 28, 105–123, doi:10.1093/hmg/ddy337.

19. Mehalow, A.K.; Kameya, S.; Smith, R.S.; Hawes, N.L.; Denegre, J.M.; Young, J.A.; Bechtold, L.; Haider, N.B.; Tepass, U.; Heckenlively, J.R.; et al. *CRB1* is essential for external limiting membrane integrity and photoreceptor morphogenesis in the mammalian retina. *Hum. Mol. Genet.* **2003**, 12, 2179–2189, doi:10.1093/hmg/ddg232.

20. van de Pavert, S.A.; Sanz sanz, A.; Aartsen, W.M.; Vos, R.M.; Versteeg, I.; Beck, S.C.; Klooster, J.; Seeliger, M.W.; Wijnholds, J. *Crb1* is a Determinant of Retinal Apical Muller Glia Cell Features. *Glia* **2007**, 1486–1497, doi:10.1002/glia.

21. Alves, C.H.; Sanz sanz, A.; Park, B.; Pellissier, L.P.; Tanimoto, N.; Beck, S.C.; Huber, G.; Murtaza, M.; Richard, F.; Sridevi gurubaran, I.; et al. Loss of *CRB2* in the mouse retina mimics human retinitis pigmentosa due to mutations in the *CRB1* gene. *Hum. Mol. Genet.* **2013**, 22, 35–50, doi:10.1093/hmg/dds398.

22. Pellissier, L.P.; Alves, C.H.; Quinn, P.M.; Vos, R.M.; Tanimoto, N.; Lundvig, D.M.S.; Dudok, J.J.; Hooibrink, B.; Richard, F.; Beck, S.C.; et al. Targeted Ablation of Crb1 and Crb2 in Retinal Progenitor Cells Mimics Leber Congenital Amaurosis. *PLoS Genet.* **2013**, *9*, doi:10.1371/journal.pgen.1003976.
23. Quinn, P.M.; Buck, T.M.; Mulder, A.A.; Ohonin, C.; Alves, C.H.; Vos, R.M.; Bialecka, M.; van Herwaarden, T.; van Dijk, E.H.C.; Talib, M.; et al. Human iPSC-Derived Retinas Recapitulate the Fetal CRB1 CRB2 Complex Formation and Demonstrate that Photoreceptors and Müller Glia Are Targets of AAV5. *Stem Cell Reports* **2019**, *12*, 906–919, doi:10.1016/j.stemcr.2019.03.002.
24. van Rossum, A.G.S.H.; Aartsen, W.M.; Meuleman, J.; Klooster, J.; Malysheva, A.; Versteeg, I.; Arsanto, J.P.; Le Bivic, A.; Wijnholds, J. Pals1/Mpp5 is required for correct localization of Crb1 at the subapical region in polarized Müller glia cells. *Hum. Mol. Genet.* **2006**, *15*, 2659–2672, doi:10.1093/hmg/ddl194.
25. Mairot, K.; Smirnov, V.; Bocquet, B.; Labesse, G.; Arndt, C.; Defoort-dhellemmes, S.; Zanlonghi, X.; Hamroun, D.; Denis, D.; Picot, M.C.; et al. Crb1-related retinal dystrophies in a cohort of 50 patients: A reappraisal in the light of specific müller cell and photoreceptor crb1 isoforms. *Int. J. Mol. Sci.* **2021**, *22*, doi:10.3390/ijms222312642.
26. Boon, N.; Lu, X.; Andriessen, C.A.; Moustakas, I.; Buck, T.M.; Freund, C.; Arendzen, C.H.; Böhringer, S.; Boon, C.J.F.; Mei, H.; Wijnholds, J. AAV-mediated gene augmentation therapy of CRB1 patient-derived retinal organoids restores the histological and transcriptional retinal phenotype. *Stem Cell Reports* **2023**, doi:https://doi.org/10.1016/j.stemcr.2023.03.014.
27. Alves, C.H.; Boon, N.; Mulder, A.A.; Koster, A.J.; Jost, C.R.; Wijnholds, J. CRB2 Loss in Rod Photoreceptors Is Associated with Progressive Loss of Retinal Contrast Sensitivity. *Int. J. Mol. Sci.* **2019**, *20*, 4069, doi:10.3390/ijms20174069.
28. Quinn, P.M.; Alves, C.H.; Klooster, J.; Wijnholds, J. CRB2 in immature photoreceptors determines the superior-inferior symmetry of the developing retina to maintain retinal structure and function. *Hum. Mol. Genet.* **2018**, *27*, 3137–3153, doi:10.1093/hmg/ddy194.
29. Alves, C.H.; Pellissier, L.P.; Vos, R.M.; Garrido, M.G.; Sothilingam, V.; Seide, C.; Beck, S.C.; Klooster, J.; Furukawa, T.; Flannery, J.G.; et al. Targeted ablation of Crb2 in photoreceptor cells induces retinitis pigmentosa. *Hum. Mol. Genet.* **2014**, *23*, 3384–3401, doi:10.1093/hmg/ddu048.
30. Assou, S.; Girault, N.; Plinet, M.; Bouckenheimer, J.; Sansac, C.; Combe, M.; Mianné, J.; Bourguignon, C.; Fieldes, M.; Ahmed, E.; et al. Recurrent Genetic Abnormalities in Human Pluripotent Stem Cells: Definition and Routine Detection in Culture Supernatant by Targeted Droplet Digital PCR. *Stem Cell Reports* **2020**, *14*, 1–8, doi:10.1016/j.stemcr.2019.12.004.

31. van de Pavert, S.A.; Meuleman, J.; Malysheva, A.; Aartsen, W.M.; Versteeg, I.; Tonagel, F.; Kamphuis, W.; McCabe, C.J.; Seeliger, M.W.; Wijnholds, J. A single amino acid substitution (Cys249Trp) in *Crb1* causes retinal degeneration and deregulates expression of pituitary tumor transforming gene *Pttg1*. *J. Neurosci.* **2007**, *27*, 564–573, doi:10.1523/JNEUROSCI.3496-06.2007.
32. Buck, T.M.; Vos, R.M.; Alves, C.H.; Wijnholds, J. AAV-CRB2 protects against vision loss in an inducible CRB1 retinitis pigmentosa mouse model. *Mol. Ther. Methods Clin. Dev.* **2021**, *20*, 423–441, doi:10.1016/j.omtm.2020.12.012.
33. Jo, H.Y.; Lee, Y.; Ahn, H.; Han, H.J.; Kwon, A.; Kim, B.Y.; Ha, H.Y.; Kim, S.C.; Kim, J.H.; Kim, Y.O.; et al. Functional in vivo and in vitro effects of 20q11.21 genetic aberrations on hPSC differentiation. *Sci. Rep.* **2020**, *10*, 1–14, doi:10.1038/s41598-020-75657-7.
34. Hallam, D.; Hilgen, G.; Dorgau, B.; Zhu, L.; Yu, M.; Bojic, S.; Hewitt, P.; Schmitt, M.; Uteng, M.; Kustermann, S.; et al. Human-Induced Pluripotent Stem Cells Generate Light Responsive Retinal Organoids with Variable and Nutrient-Dependent Efficiency. *Stem Cells* **2018**, *36*, 1535–1551, doi:10.1002/stem.2883.
35. Pellissier, L.P.; Hoek, R.M.; Vos, R.M.; Aartsen, W.M.; Klimczak, R.R.; Hoyng, S.A.; Flannery, J.G.; Wijnholds, J. Specific tools for targeting and expression in Müller glial cells. *Mol. Ther. - Methods Clin. Dev.* **2014**, *1*, 14009, doi:10.1038/mtm.2014.9.
36. Warlich, E.; Kuehle, J.; Cantz, T.; Brugman, M.H.; Maetzig, T.; Galla, M.; Filipczyk, A.A.; Halle, S.; Klump, H.; Schöler, H.R.; et al. Lentiviral vector design and imaging approaches to visualize the early stages of cellular reprogramming. *Mol. Ther.* **2011**, *19*, 782–789, doi:10.1038/mt.2010.314.
37. Zhong, X.; Gutierrez, C.; Xue, T.; Hampton, C.; Vergara, M.N.; Cao, L.H.; Peters, A.; Park, T.S.; Zambidis, E.T.; Meyer, J.S.; et al. Generation of three-dimensional retinal tissue with functional photoreceptors from human iPSCs. *Nat. Commun.* **2014**, *5*, doi:10.1038/ncomms5047.
38. Wang, Q.; Liu, J.; Janssen, J.M.; Le Boutejller, M.; Frock, R.L.; Gonçalves, M.A.F.V. Precise and broad scope genome editing based on high-specificity Cas9 nickases. *Nucleic Acids Res* **2021** *49*, 1173-1198.
39. Clement, K.; Rees, H.; Canver, M.C.; Gehrke, J.M.; Farouni, R.; Hsu, J.Y.; Cole, M.A.; Liu, D.R.; Joung, J.K.; Bauer, D.E.; Pinello, L. CRISPResso2 provides accurate and rapid genome editing sequence analysis. *Nat Biotechnol* **2019** *37*, 224-226.

Supplemental information

Supplemental Table 1. hiPSC line information (Applied Stem Cell, California, USA), related to Supplemental Figure 1.

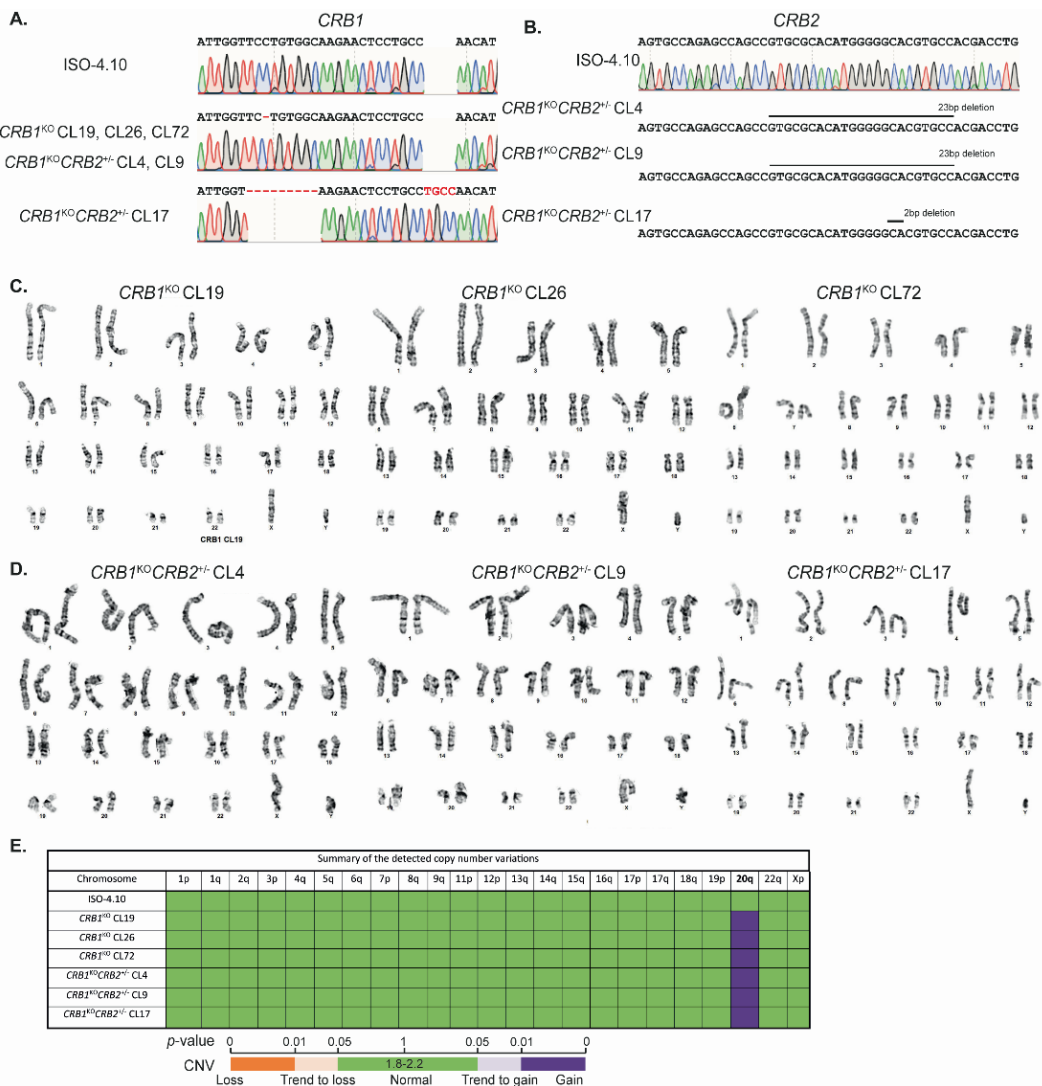
Previously published	Description	Gender
LUMC04iCTRL10 [23]	<u>ISO-4.10</u> = Isogenic control	Male
NA	<u>CRB1^{KO} CL19</u> = homozygous c.500del; p.(Ser44Serfs*)	Male
NA	<u>CRB1^{KO} CL26</u> = homozygous c.500del; p.(Ser44Serfs*)	Male
NA	<u>CRB1^{KO} CL72</u> = homozygous c.500del ; p.(Ser44Serfs*)	Male
NA	<u>CRB1^{KO}CRB2^{+/-} CL4</u> = CRB1: homozygous c.500del ; p.(Ser44Serfs*), CRB2: heterozygous mutation targeting exon3.	Male
NA	<u>CRB1^{KO}CRB2^{+/-} CL9</u> = CRB1: homozygous c.500del ; p.(Ser44Serfs*), CRB2: heterozygous mutation targeting exon3.	Male
NA	<u>CRB1^{KO}CRB2^{+/-} CL17</u> = CRB1: homozygous c.498_507delinsTGCC; p.(Ser44Lysfs*), CRB2: heterozygous mutation targeting exon3.	Male

Supplemental Table 2. PCR primer sequences for confirmation of mutations.

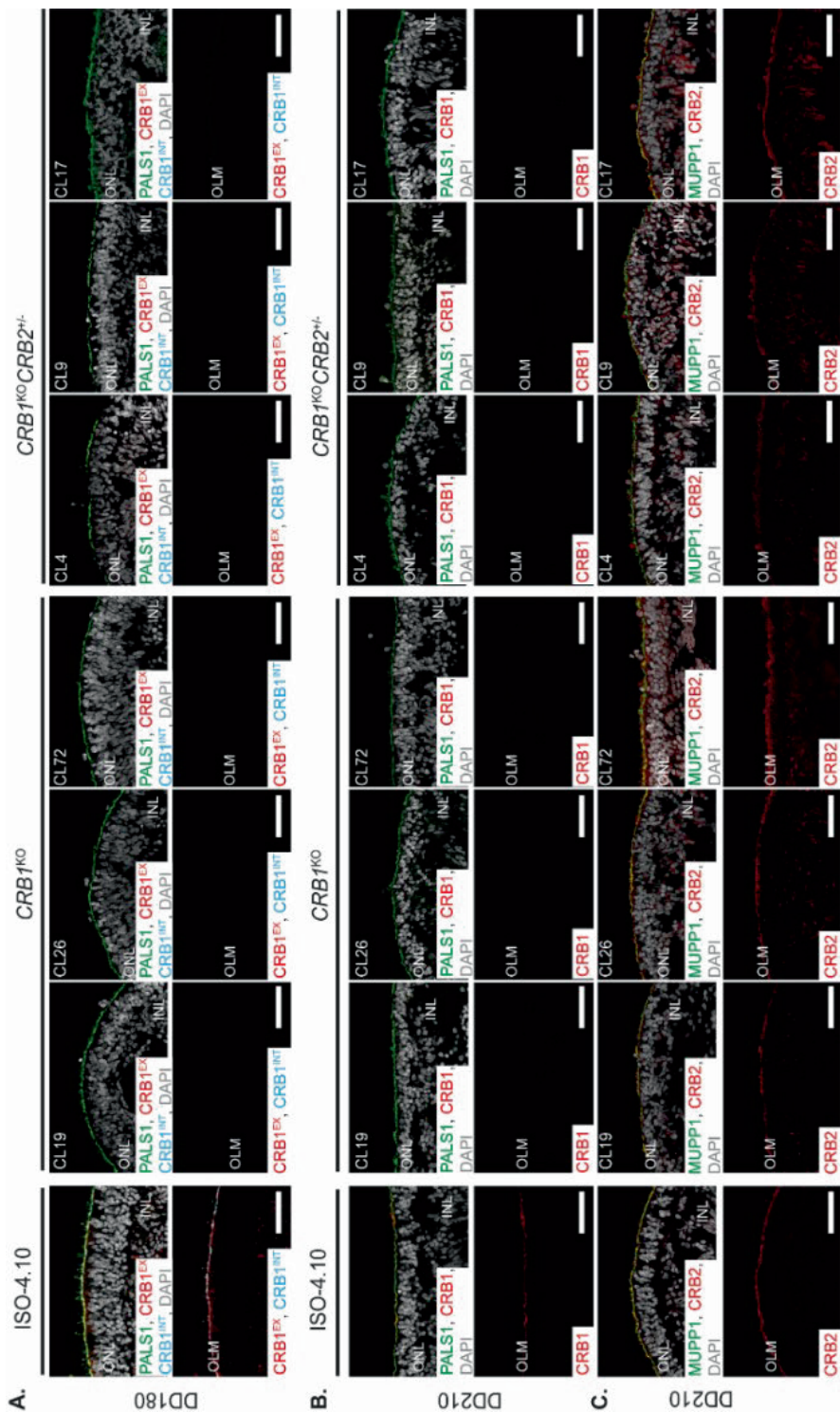
Target	PCR primers	
<i>CRB1</i>	FW	GACAATGATTGTTCTTGTTTCAGACACAGCC
	REV	CATCCACTTCCAAGTCGCAGTGTC
Sanger sequencing primers		
<i>CRB1</i>	FW	GGACAAAGACTGTGACAACATGAAAGACC
	REV	GGACACAGAAGCAGGAGTAACCATC
Target	NGS primers (5' to 3') (Illumina adapter overhang)	
<i>CRB2</i>	FW	GATGTGTATAAGAGACAGGTGCCATCCTGCACCCTGTG
	REV	CGTGTGCTCTCCGATCTTCGCTACCCGTTGACCAGGT

Supplemental Table 3. Barcode PCR primers used in the NGS amplicon sequence analysis.

Barcode name	Primer Sequence (5' to 3')	Barcode in primer	Read in Miseq
719	CAAGCAGAAGACGGCATAACGAGAT TACTACGC GTGACTGGAGTTCAGACGTGT GCTCTTCCGATCT	TACTACGC	TACTACGC
720	CAAGCAGAAGACGGCATAACGAGAT AGGCTCCG GTGACTGGAGTTCAGACGTGT GCTCTTCCGATCT	AGGCTCCG	AGGCTCCG
721	CAAGCAGAAGACGGCATAACGAGAT GCAGCGTA GTGACTGGAGTTCAGACGTGT GCTCTTCCGATCT	GCAGCGTA	GCAGCGTA
722	CAAGCAGAAGACGGCATAACGAGAT GAGCGCTA GTGACTGGAGTTCAGACGTGT GCTCTTCCGATCT	GAGCGCTA	GAGCGCTA
508	AATGATACGGCGACCACCGAGATCTACAC GTACTGAC TCGTCGGCAGCGTCAGATGTG TATAAGAGACAG	GTACTGAC	GTACTGAC



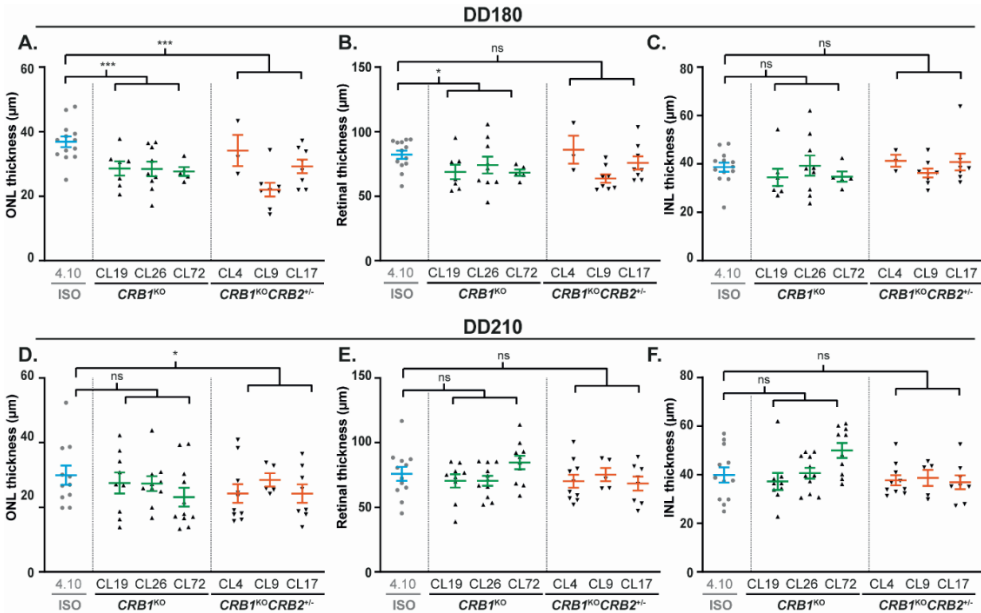
Supplemental Figure 1: Confirmation of mutations and condition of $CRB1^{KO}$ and $CRB1^{KO}CRB2^{+/-}$ hiPSC. Related to all figures. (A) Confirmation of the homozygous $CRB1$ mutation in $CRB1^{KO}$ and $CRB1^{KO}CRB2^{+/-}$ hiPSC using Sanger sequencing, with $CRB1^{KO}CRB2^{+/-}$ CL17 containing a distinct mutation. (B) Confirmation of the heterozygous $CRB2$ mutation in $CRB1^{KO}CRB2^{+/-}$ hiPSC using Sanger Sequencing and Next Generation Sequencing (C, D) Karyotyping results of (C) $CRB1^{KO}$ and (D) $CRB1^{KO}CRB2^{+/-}$ hiPSC. (E) Meta-analysis of 90% most recurrent abnormalities in hiPSCs showing a gain in copy number variation (CNV) in chromosome 20q for hiPSC used in this study.



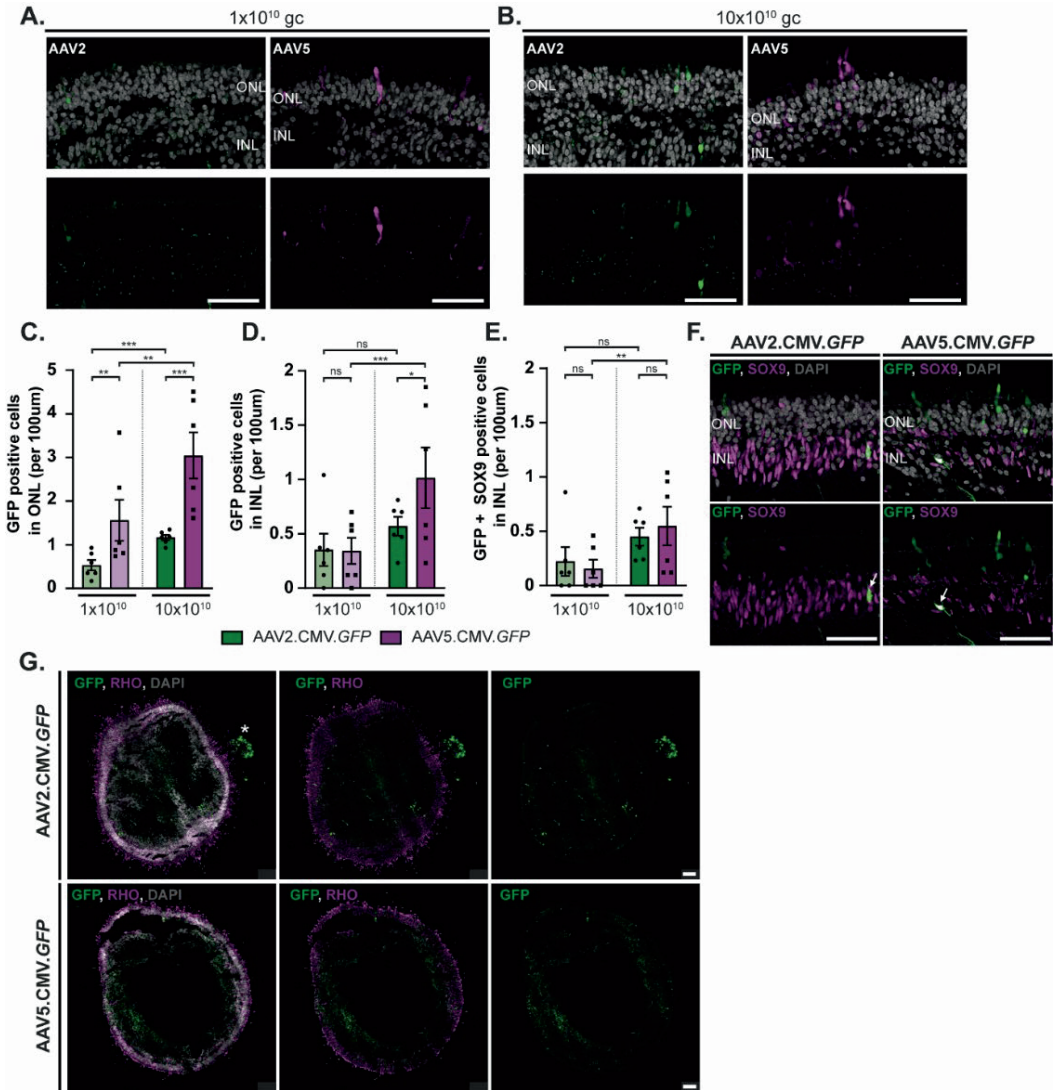
Supplemental Figure 2: CRB1 is absent in DD180 and DD210 $CRB1^{KO}$ and $CRB1^{KO}CRB2^{+/-}$ retinal organoids. Related to Figure 2.

Legend continues on the next page.

Representative immunohistochemical images of three *CRB1*^{KO} and three *CRB1*^{KO}*CRB2*^{+/-} retinal organoids compared to the isogenic control at DD180 and DD210. (A) DD180 organoids expressing PALS1 (green) in all retinal organoids at the OLM and *CRB1*^{EX} (red), and *CRB1*^{INT} (cyan) was only detected in the isogenic control. (B) DD210 retinal organoids stained with PALS1 (green) and *CRB1* (red), similar as observed in DD180. (C) MUPP1 (green) and *CRB2* (red) is expressed at the OLM in control, *CRB1*^{KO}, and *CRB1*^{KO}*CRB2*^{+/-} retinal organoids at DD210. Note: INL = Inner Nuclear Layer, ONL = Outer Nuclear Layer, OLM = Outer Limiting Membrane. Scalebar = 50µm.

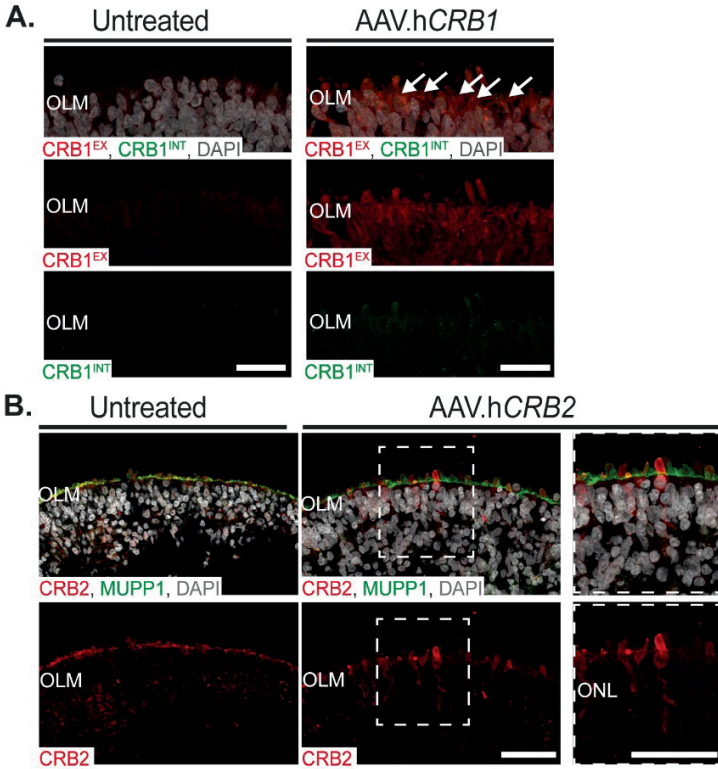


Supplemental Figure 3: Additional phenotype quantifications of DD180 and DD210 *CRB1*^{KO} and *CRB1*^{KO}*CRB2*^{+/-} retinal organoids. (A, B, C) Quantification of the (A) ONL, (B) retinal, and (C) INL thickness of DD180 retinal organoids. (D, E, F) Quantification of the (D) ONL, (E) retinal, and (F) INL thickness of DD210 retinal organoids. Each datapoint in the graph represents an individual organoid, of which an average has been taken of 3-6 representative images. The SEM is derived from these averages. Number of individual organoids used for the quantification per condition at DD180: 4.10 $n=14$, *CRB1*^{KO} CL19 $n=7$, CL26 $n=5$, CL72 $n=9$, *CRB1*^{KO}*CRB2*^{+/-} CL4 $n=3$, CL9 $n=8$, CL17 $n=8$; and DD210: 4.10 $n=12$, *CRB1*^{KO} CL19 $n=9$, CL26 $n=10$, CL72 $n=11$, *CRB1*^{KO}*CRB2*^{+/-} CL4 $n=8$, CL17 $n=8$ from at least two independent differentiation batches and *CRB1*^{KO}*CRB2*^{+/-} CL9 $n=5$ from one differentiation batch. Statistical analysis: generalized linear mixed models with $p < 0.05$ (*), $p < 0.01$ (**), and $p < 0.001$ (***)

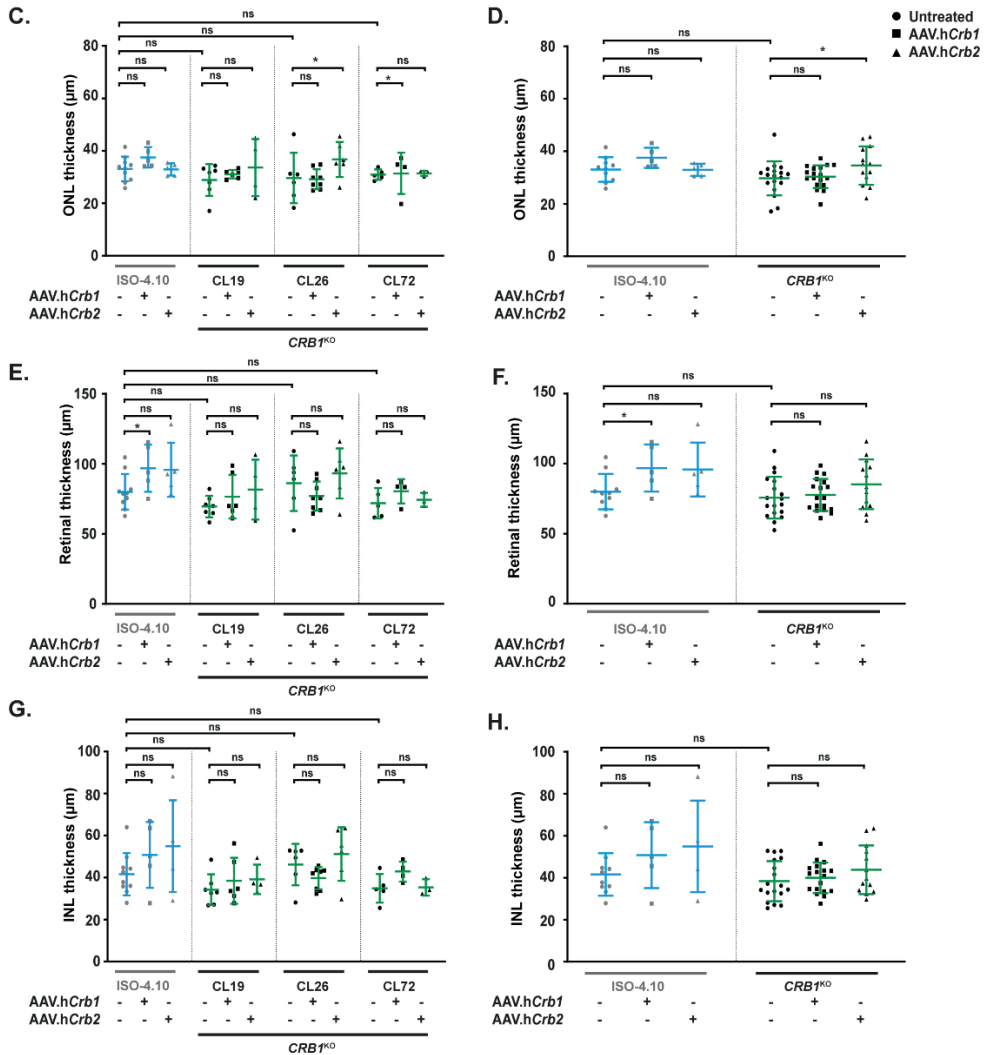


Supplemental Figure 4: AAV transduction study of control retinal organoids transduced at DD200 with AAV2.CMV.GFP or AAV5.CMV.GFP (A, B) Representative immunohistochemical images of control retinal organoids transduced with (A) 1x10¹⁰gc, or (B) 10x10¹⁰gc AAV2.CMV.GFP or AAV5.CMV.GFP. (C,D, E) Quantification of the number of GFP positive cells in the (D) ONL, (E) INL, and (F) GFP positive and co-localized with SOX9 in the INL (marking MGCs). Statistical analysis was performed within the same AAV capsid (dose-dependent) or within the same AAV titer (comparing AAV2 with AAV5 transduction efficiency). (F, G) Immunohistochemical images of co-localization of AAV.GFP with MGC marker SOX9 (F) and photoreceptor cell marker Rhodopsin (RHO) (G). Arrows indicate

colocalization of SOX9 with GFP (F), and the asterisk indicates the retinal pigment epithelium (G). Each datapoint in the graph represents individual organoids, of which an average has been taken of 3-6 representative images. The SEM is derived from these averages. Number of individual organoids used for quantification per condition for AAV2.CMV.GFP: 1×10^{10} gc $n = 6$, 10×10^{10} gc $n = 6$; and for AAV5.CMV.GFP: 1×10^{10} gc $n = 6$, 10×10^{10} gc $n = 6$ from one differentiation bath. Note: INL = Inner Nuclear Layer, ONL = Outer Nuclear Layer. Scalebar = $50 \mu\text{m}$, statistical analysis: generalized linear mixed models with $p < 0.05$ (*), $p < 0.01$ (**), and $p < 0.001$ (***)



Supplemental Figure 5 (A-B): AAV-mediated gene therapy on *CRB1*^{KO} organoids. (A, B) representative immunohistochemical image of (A) CRB1 in untreated and AAV.hCRB1 and (B) CRB2 in untreated and AAV.hCRB2 treated *CRB1*^{KO} retinal organoids.



Supplemental Figure 5 (C-H): AAV-mediated gene therapy on $CRB1^{KO}$ organoids. (C, D, E, F, G, H) Quantification of the (C, D) ONL thickness, (E, F) the retinal thickness, and (G, H) INL thickness per $CRB1^{KO}$ clone (C, E, G) or all $CRB1^{KO}$ clones combined (D, F, H). Each datapoint in the graph represents individual organoids, of which an average has been taken of at least three representative images. The SEM is derived from these averages. Number of individual organoids used for quantification per condition for untreated: 4.10 $n = 10$, $CRB1^{KO}$ CL19 $n = 7$, CL26 $n = 7$, CL72 $n = 5$; AAV.hCrb1 treated: 4.10 $n = 5$, $CRB1^{KO}$ CL19 $n = 6$, CL26 $n = 8$, CL72 $n = 4$ from two independent differentiation batches; and AAV.hCrb2 treated: 4.10 $n = 5$, $CRB1^{KO}$ CL19 $n = 4$, CL26 $n = 6$, CL72 $n = 3$ from one differentiation batch. Note: ONL = Outer Nuclear Layer, OLM = Outer Limiting Membrane. Scalebar = $50\mu\text{m}$, statistical analysis: generalized linear mixed models with $p < 0.05$ (*), $p < 0.01$ (**), and $p < 0.001$ (***)